ELSEVIER

Surface Science 459 (2000) 173–182

surface science

www.elsevier.nl/locate/susc

Fermi surface contours of p(2 × 2)O/Mo(110): an angle-resolved photoelectron spectroscopy study

Jörg Kröger [1,*], Thomas Greber, Jürg Osterwalder

Physik-Institut der Universität Zürich, Winterthurerstraße 190, CH-8057 Zürich, Switzerland

Received 7 January 2000; accepted for publication 1 April 2000

Abstract

We present the Fermi surface map of p(2 × 2)O/Mo(110) at room temperature. Changes with respect to the clean surface are discussed. Three surface-state contours ('hole pockets') that exist on the clean surface are found to persist on the oxygen-covered surface with slightly changed volumes. The large 'electron pocket' shows no significant shift. In combination with a previous electron energy-loss spectroscopy experiment measuring the surface phonon dispersion curves, these data put into question the recently postulated driving force for stabilizing the p(2 × 2) superstructure in the low-coverage regime. © 2000 Elsevier Science B.V. All rights reserved.

Keywords: Angle resolved photoemission; Low index single crystal surfaces; Molybdenum; Photoelectron diffraction; Photoelectron emission; Surface electronic phenomena (work function, surface potential, surface states, etc.)

1. Introduction

From the hydrogen-saturated Mo(110) surface is it known that adsorbate-induced giant Kohn anomalies exist both for the transverse and the longitudinal acoustic surface phonon modes [1–5] which we refer to as the Rayleigh wave and the longitudinal mode, respectively. A giant Kohn anomaly is characterized by a significant lowering of the energy of a (surface) phonon mode at a critical wave vector. In the dispersion curves of the corresponding phonon modes this anomaly exhibits deep indentations. These pronounced anomalies can be related to quasi-one-dimensional Fermi surface nesting as is deduced both from theory [6–9] and experiment [10]. By quasi-one-dimensional Fermi surface nesting one refers to a characteristic shape of the Fermi surface of surface states; i.e., it consists of contours that reveal parallel segments in an extended region in *k*-space. It turns out that the nesting vectors, i.e., the vectors in reciprocal space that span the parallel regions, equal the critical wave vectors of the phonon modes which suffer the giant Kohn anomaly. Apart from analysing the prerequisites for a giant Kohn anomaly, it is interesting to know if hydrogen plays an exclusive role concerning the adsorbate-induced anomaly or if other adsorbates are able to cause similar anomalies. An earlier experiment by means of angle-resolved photoelectron spectroscopy discovered large nested segments in the Fermi surface contours of p(2 × 2)O/Mo(110) [11,12]. In fact, the Fermi surface was found to consist of hole pockets, i.e., contours that enclose unoccupied surface states,

* Corresponding author. Fax: +39-40-375-8400.

E-mail address: kroegerj@elettra.trieste.it (J. Kröger)

[1] Present address: APE-Beamline, INFM, c/o Lab. ELETTRA Sincrotrone Trieste, S.S. 14 Km 163.5, I-34012 Basovizza Trieste, Italy.

PII: S0039-6028(00)00480-5

which are centred in the (2×2) superlattice Brillouin zones. Since both of these pockets are of nearly the same size and shape, they can be coupled entirely to each other by global nesting vectors that coincide with the $\bar{S}$ and $\bar{N}$ points of the surface Brillouin zone. It was speculated that this nesting provides a purely electronic driving force for producing the (2×2) ordering pattern at a coverage of 0.25 monolayers (ML) for O/Mo(110). More recently, an electron energy-loss experiment was performed in order to detect possible phonon anomalies that might be expected as a further consequence of this strong nesting [5,13,14]. In these experiments no anomalies of the discussed type could be observed at the wave vectors that equal the mentioned nesting vectors, nor at other wave vectors where some degree of nesting might be deduced from the data of Refs. [11,12]. In fact, comparing the entire dispersion curves of the Rayleigh wave and the longitudinal mode for the clean surface and the $p(2\times2)O$ system, no changes could be reported. This negative result raised the question of how far the observation of Fermi surface nesting in a photoemission experiment can be used to predict anomalies in the lattice dynamics of a surface. A giant Kohn anomaly is the reaction of the system under investigation to the quasi-one-dimensional Fermi surface nesting provided that, firstly, the regions of equal curvature of the Fermi surface contours are sufficiently extended in reciprocal space and, secondly, the coupling between electronic and ionic systems is sufficiently strong.

Let us briefly review some general aspects of the adsorbate system O/Mo(110). Using low-energy electron diffraction, the existence of a $p(2\times2)$ superstructure at a coverage of 0.25 ML and at room temperature was reported [15]. For coverages slightly above 0.3 ML more complex diffraction patterns, which consist of a coverage-dependent number of satellite spots around the substrate diffraction spots, were observed. It was further shown that even at very low coverages ($\approx$0.02 ML) the $p(2\times2)O$ islands already exist. By means of electron energy-loss spectroscopy it was found that oxygen adsorbs atomically in the long bridge for coverages up to 0.25 ML. For higher coverages, a conversion of the adsorption site to the triply coordinated hollow site is observed [5,13,16].

In this publication we re-examine the system $p(2\times2)O/Mo(110)$ by angle-resolved photoelectron spectroscopy and use the convenient technique of Fermi surface mapping in order to get the complete Fermi surface of surface localized states within the first surface Brillouin zone. Our experiment, unlike the previous photoemission analysis [11,12], leads to results that do not suggest Fermi surface nesting.

2. Experimental

All experiments were performed in a modified Vacuum Generators Escalab 220 spectrometer [17] at a base pressure of less than 1×10^{-8} Pa. The pass energy of the 180° hemispherical analyser was set to 1 eV in order to achieve an energy resolution of 35 meV full-width at half-maximum for all ultraviolet photoemission experiments. The iris aperture of the input lens system was chosen to give an angular resolution of less than 1° full-width at half-maximum. Monochromatized He Iα radiation (21.2 eV) from a microwave-driven high-intensity helium discharge lamp (Gammadata VUV 5000) was used for excitation. In order to calibrate the position of the Fermi energy in molybdenum, the spectrum of a polycrystalline silver sample was recorded around the Fermi edge in a preceding experiment.

The (110) surface of the molybdenum single crystal was cut and polished to within 0.3° of the desired orientation. Before installing it into the ultrahigh vacuum chamber, the sample was heated to 1300 K in a hydrogen atmosphere for several hours.

The cleaning procedure as modelled after Refs. [18,19] consisted of several oxidation cycles where the crystal, being constantly heated to 1400 K, was exposed to oxygen for 10 min and then left without oxygen for 10 min. The oxygen pressure was chosen to be 4×10^{-6} Pa. Typically, at the end of three cycles, the crystal was flashed to 2000 K by electron bombardment of its back side. After obtaining a clean surface by this procedure it was sufficient to apply only a flash to 2000 K for

surface cleanliness. A well-prepared surface was monitored by low-energy electron diffraction, ultraviolet photoelectron spectroscopy and X-ray photoelectron spectroscopy.

For oxygen adsorption we exposed the sample to oxygen of 99.998% purity by backfilling the vacuum chamber to 1×10^{-7} Pa. The coverage was checked by low-energy electron diffraction, which yielded a sharp (2×2) diffraction pattern, and by X-ray photoelectron spectroscopy. For all experiments the crystal was at room temperature.

Concerning the explanation of the photoemission data-acquisition modes used in this experiment, i.e., Fermi surface mapping and angle-scanned energy distribution curves, the reader is referred to Refs. [20,21].

3. Results and discussion

Let us begin the presentation of our results by characterizing the clean and the $p(2\times2)O$-covered Mo(110) surface. Fig. 1a shows the main changes in the normal emission ultraviolet photoelectron spectra. The peak at ≈1.3 eV, which was assigned to be a spin–orbit-induced surface resonance [22], shifts slightly to ≈1.4 eV electron binding energy and decreases in intensity by $\approx50\%$. The weak and broad spectral feature around ≈4.9 eV in the clean case shifts to ≈4.2 eV for the $p(2\times2)O$ surface. This shift was also observed with hydrogen adsorption [10,22]. The gradual transition of these spectra with increasing oxygen exposure is demonstrated in Fig. 1b. For an exposure of 0.32 L [1 Langmuir (L) $=10^{-6}$ Torr s] a small spectral feature at ≈3.1 eV is observed which may be due to hydrogen coadsorption [10].

Fig. 2 is dedicated to the comparison of the Fermi surface maps of clean Mo(110) and $p(2\times2)O$/Mo(110). For both data sets the following procedure was adopted [17,20]. We tilted the crystal such as to measure photoemission 50° away from the surface normal, which corresponds to a parallel wave vector of the emitted photoelectrons of ≈1.6 Å^{-1}. For each polar angle between 50° and 0° (corresponding to normal emission), with a step size of 2°, the sample was rotated by 360° around its surface normal. The step size for the latter azimuthal rotation was chosen such as to obtain a homogeneous data point density. This procedure results in a total amount of 1898 data points. For each data point a sample time of 1 s was used for recording the photoelectron count at the Fermi energy ($\Delta E=$ 35 meV). The plots are in $k_{\|}$ projection with intensities represented on a logarithmic grey scale in order to enhance the weaker surface-state features (white and black represent large and small intensities, respectively). We included the bound-

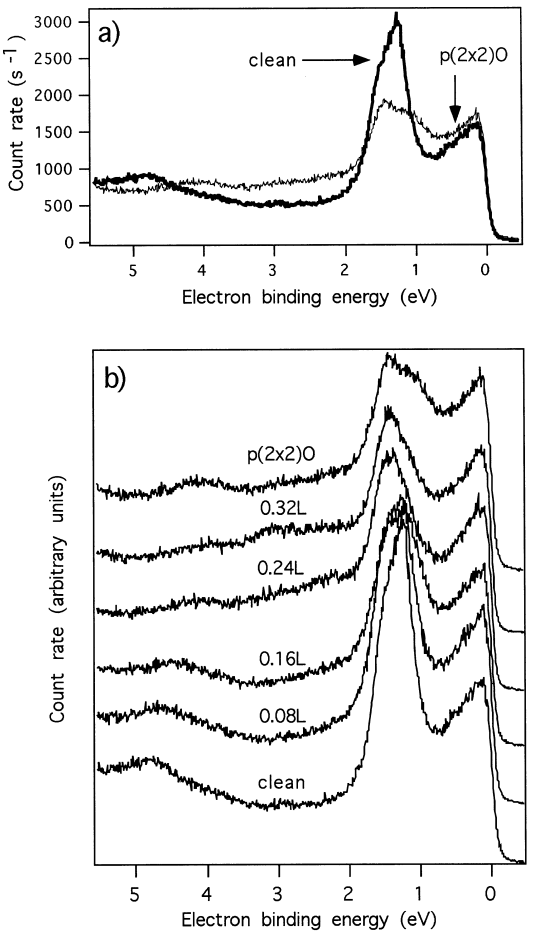

Fig. 1. (a) Normal ultraviolet photoemission spectra for the clean Mo(110) crystal and the $p(2\times2)O$ system. (b) Development of energy spectra with increasing oxygen exposure. All data were taken using monochromatized He I excitation.

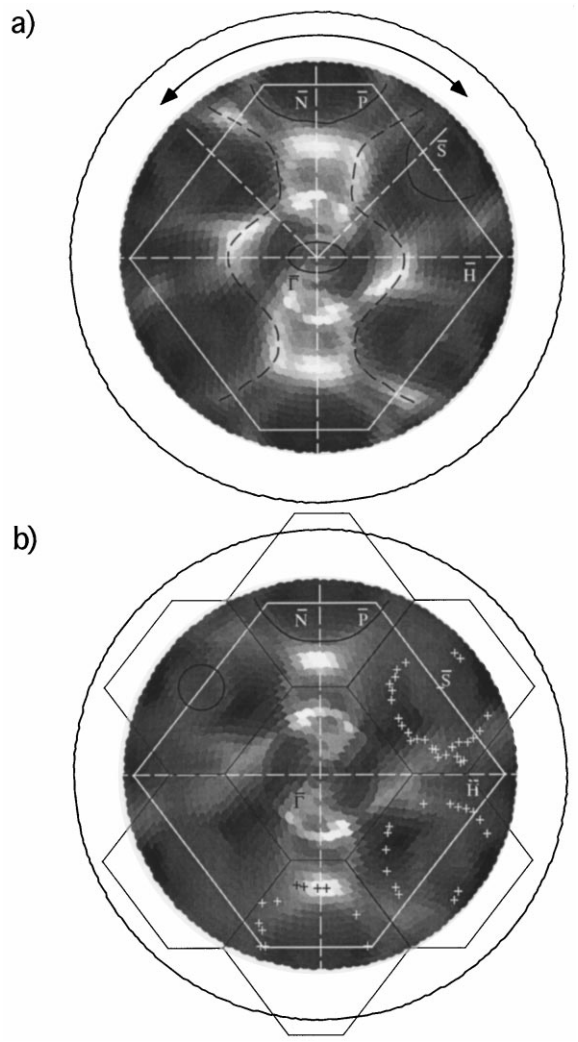

Fig. 2. (a) He I excited Fermi surface map for clean Mo(110) at room temperature. We added the first surface Brillouin zone whose boundaries are depicted as full white lines and a 90° sector around $\bar{N}$ whose boundaries are shown as dashed white lines. This sector will be investigated in more detail. The hole pockets and the electron pocket are marked as full and dashed black curves, respectively. (b) He I excited Fermi surface map for $p(2\times2)$O/Mo(110) at room temperature. The boundaries of the first surface Brillouin zone and the (2×2) surface Brillouin zones are shown as full white and full black lines, respectively. The hole pockets around $\bar{N}$ and $\bar{S}$ are presented as full black curves. Some of the data of a previous photoemission experiment are included as small crosses (data taken from [11]).

aries of the first surface Brillouin zone (full white lines) for locating features in reciprocal space and for a definition of the symmetry points $\bar{\Gamma}$, $\bar{H}$, $\bar{N}$, $\bar{P}$ and $\bar{S}$. In Fig. 2b we also show the $p(2\times2)$ adsorbate Brillouin zones (full black lines).

The Fermi surface map of the clean surface (Fig. 2a) is in good agreement with the results of a previous angle-resolved photoemission experiment [18]. We find the same surface-state hole pockets around $\bar{\Gamma}$, $\bar{N}$ and $\bar{S}$, and an irregular electron pocket that extends along the $\bar{\Gamma}\bar{N}$ direction ($[1\bar{1}0]$), the topology of which is not fully clear at this point [7,10,18]. All contours are highlighted as full (hole pockets) and dashed (electron pocket) black lines. In addition, various bulk-related Fermi surface contours are observed that are characterized by showing almost no sensitivity upon adsorption. In the Fermi surface maps they can be seen as bright features that stay fixed in reciprocal space upon oxygen adsorption. These bulk states were characterized completely by Jeong et al. [22] and our results are in good agreement.

Fig. 2b shows the corresponding Fermi surface map of the $p(2\times2)$O superstructure at 0.25 ML oxygen coverage. At first glance the changes between the two data sets are small. One observes an overall decrease in intensity and a broadening of some contours. In contrast to the scenario described by Dhar et al. [11], where the electron pocket of the clean surface shifts towards the surface Brillouin zone boundary and coalesces with its counterpart in the second surface Brillouin zone, we do not find the resulting elliptical hole pockets indicated by small crosses in Fig. 2b. Even at higher and lower oxygen coverages we could not reproduce the Fermi surface contours of Dhar et al. [11]. Instead, we still recognize the hole pocket centred at the $\bar{S}$ point which has shrunk considerably. The $\bar{N}$-centred hole pocket is only slightly contracted. The two contours have thus strongly different volumes and shapes. No significant shifts can be assigned to the electron pocket.

In order to refine the picture we got from Fig. 2, we performed supplemental measurements: (1) we measured only a part of the complete Fermi surface map (see the sector indicated in Fig. 2a, the boundaries of this 90° sector around $\bar{N}$ are depicted as dashed white lines, note also the arc at the top of the Fermi surface map) using better statistics and an enhanced density of data points; (2) we analysed the energy dispersion of the bands, watching

for energy shifts due to oxygen exposure; and (3) we monitored the development of the Fermi surface contours with increasing oxygen coverage starting from the clean surface up until the p(2×2)O superstructure was established at its maximum intensity and just before new extra spots developed in the low-energy electron diffraction pattern. For point (1) of our additional investigation we selected a region within the Fermi surface map where a shift of the electron pocket contour should be clearly visible. According to Dhar et al., the electron pocket (highlighted as a dashed black line in Fig. 2a) should shift along [001] ($\bar{\Gamma}\bar{H}$ direction) upon oxygen adsorption. This shift would be clearly visible in the marked sector of the Fermi surface map because of a large part of this contour is contained. Moreover, we know from our work on H/Mo(110) [10] that upon hydrogen adsorption the electron pocket becomes clearly distinct from a bulk band due to its shift towards the surface Brillouin zone boundary. The bulk band is also contained in this sector. Figs. 3 and 4 show the results for the clean surface and for p(2×2)O/Mo(110) at 0.25 ML, respectively. For measuring this sector we rotated the emission direction 45° out of the surface normal and chose the azimuthal angle to cover an interval of 90°. The step in the polar angle was set to 1° and the sampling time was chosen to be 2 s. Comparing the data sets in Figs 3a and 4a one finds that, apart from a broadening of the contours and a general decrease of the intensities, the shape of the contours is only weakly affected by oxygen adsorption. To confirm that the contours shown mark Fermi-level crossings of electronic bands, we recorded an angle-scanned collection of energy distribution curves along the azimuthal line indicated (dashed white line). For these data sets (displayed in Figs. 3b and 4b) the azimuthal angle covers a 90° interval in steps of 1.5°. The radius corresponds to a parallel wave vector of $\approx 0.7\,\text{Å}^{-1}$. Each energy distribution curve runs from -450 meV to 1050 meV electron binding energy in steps of 10 meV. In order to locate the Fermi-level crossings precisely, angular distribution curves were recorded at the Fermi edge (see Figs. 3c and 4c). These curves are horizontal cuts in the presented angle-scanned collection of energy

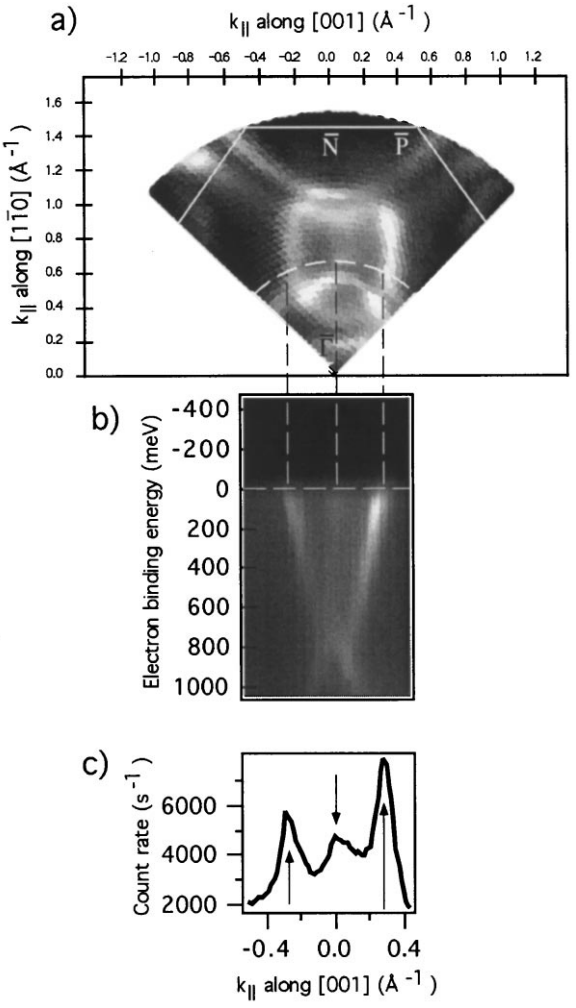

Fig. 3. (a) Part of the Fermi surface map of clean Mo(110) shown in Fig. 2a using a larger sampling time and an enhanced density of data points. (b) Angle-scanned energy distribution curves recorded along the dashed line indicated in (a). This clearly shows that the contours observed in (a) belong to Fermi-level crossings of electronic bands. (c) Angular distribution curve recorded at the Fermi edge [indicated as a dashed line in (b)].

distribution curves at a chosen energy, in our case at the Fermi energy. Within the precision of our experiment we find no shift of the main feature at $k_{\parallel} = \pm 0.27\,\text{Å}^{-1}$ (see upward pointing arrows in Figs. 3c and 4c). As was found earlier [10,23], there is a bulk band crossing the Fermi level at just these positions when measured at a photon

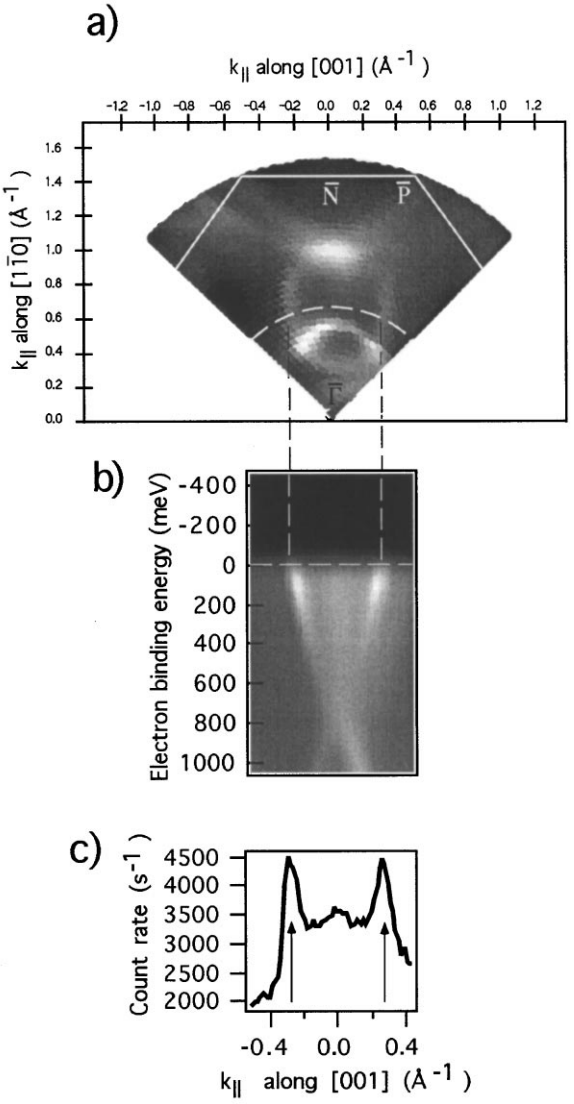

Fig. 4. Analogous to Fig. 3 for p(2×2)O/Mo(110).

energy of 21.21 eV on Mo(110). On the clean surface this bulk band is very close to the surface-state electron pocket contour, and the two states cannot be resolved individually. They can, however, be separated well by hydrogen adsorption [10] or by lithium adsorption [23], in which cases the surface state shifts by a significant amount in momentum space. Here, no change is observed except for a pile-up of diffuse intensity outside the bulk band region. This diffuse intensity is distributed asymmetrically with respect to the high-symmetry direction ($\bar{\Gamma}\bar{N}$) of the Mo(110) surface. The oblique photon incidence geometry in our experiment [17] may cause such asymmetries due to photon polarization effects in the photoemission matrix elements. Another bulk band is located on the $\bar{\Gamma}\bar{N}$ direction (see downward pointing arrow at 0 Å^{-1}).

With regard to point (2), we show in Figs. 5 and 6 the band dispersion for the clean and the p(2×2)O-covered surface (0.25 ML) measured along the $\bar{\Gamma}\bar{H}$ ([001]) and the $\bar{\Gamma}\bar{N}$ ([1$\bar{1}$0]) directions of the surface Brillouin zone, respectively. The data sets labelled (a) and (b) are collections of energy distribution curves where one spectrum was measured every 1.5° in polar angle. In the regions of momentum space covered by these figures, the oxygen-induced changes to the observed bands are more apparent. Along the $\bar{\Gamma}\bar{H}$ direction (Fig. 5) the clean surface exhibits one strong band that crosses the Fermi level (E_F) at a polar angle of $\approx 20°$, corresponding to $k_{\parallel} \approx 0.71$ Å^{-1}. This crossing is seen as a strong peak in the intensity scan taken at E_F (Fig. 5c), i.e., along the dashed line in Fig. 5a. The data from the p(2×2)O surface show this peak to be reduced by a factor of almost two, with a slight splitting near E_F, and with strong side bands on the high-momentum side. This adsorbate sensitivity characterizes this band as a surface state: it forms part of the electron pocket discussed earlier. Similar splittings have been observed on the same surface state upon lithium adsorption [23], where it was assigned to adsorbate-enhanced spin–orbit interaction. We have no explanation for the strong side bands. The sample showed a sharp (2×2) LEED pattern, making the conjecture of several coexistent phases unlikely. These data make it clear that the electron pocket has not coalesced with its partners in the neighbouring Brillouin zones to form new hole pockets around the $\bar{S}$ points, as was suggested by the data of Dhar et al. [11].

Again, quite strong spectral changes with oxygen adsorption occur along the $\bar{\Gamma}\bar{N}$ direction (Fig. 6). The dispersion of the bands here is extremely fast such that the angular sampling

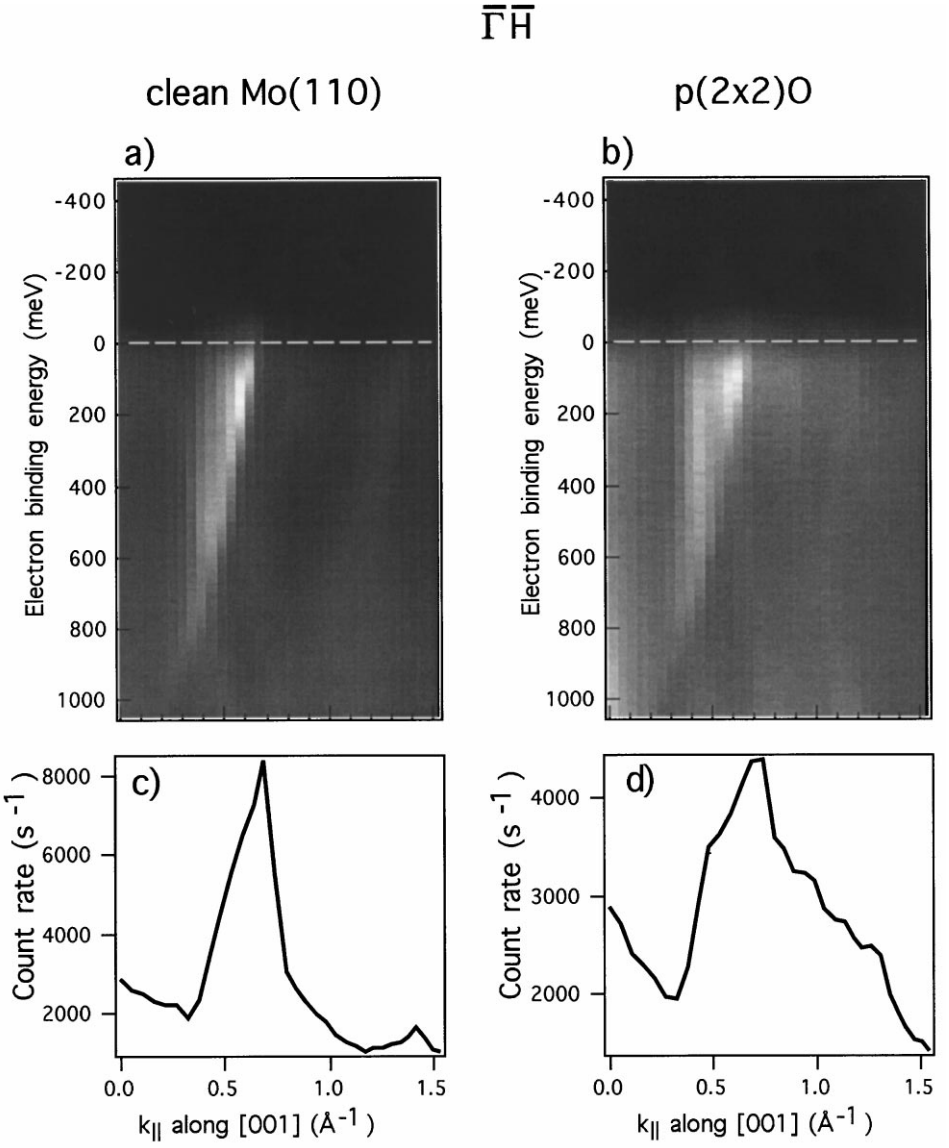

Fig. 5. (a) Polar-angle-scanned energy distribution curves along $\bar{\Gamma}\bar{H}$ ([001]) for clean Mo(110). (b) Completely analogous to (a) for p(2×2)O/Mo(110). (c) Angle distribution curve recorded at the Fermi level [indicated as a dashed line in (a)]. (d) As (c) for p(2×2)O/Mo(110).

density of 1.5° steps is just barely sufficient to follow the individual bands. The band closest to the surface normal ($k_{\parallel}=0$) is associated with the hole pocket centred at the $\bar{\Gamma}$ point on the clean surface. It broadens in energy (Fig. 6b) but seems to cross the Fermi level at essentially the same position. The strong band crossing E_F at a polar angle of $\approx 14°$, corresponding to $k_{\parallel}\approx 0.50$ Å^{-1}, is due to a bulk band and is only weakly affected upon oxygen adsorption. Between the polar angles $\approx 20°$ and $\approx 30°$, corresponding to parallel k-vectors of ≈ 0.71 Å^{-1} and ≈ 1.03 Å^{-1}, respectively, we find a band that splits into two just below E_F. The higher-momentum feature forms

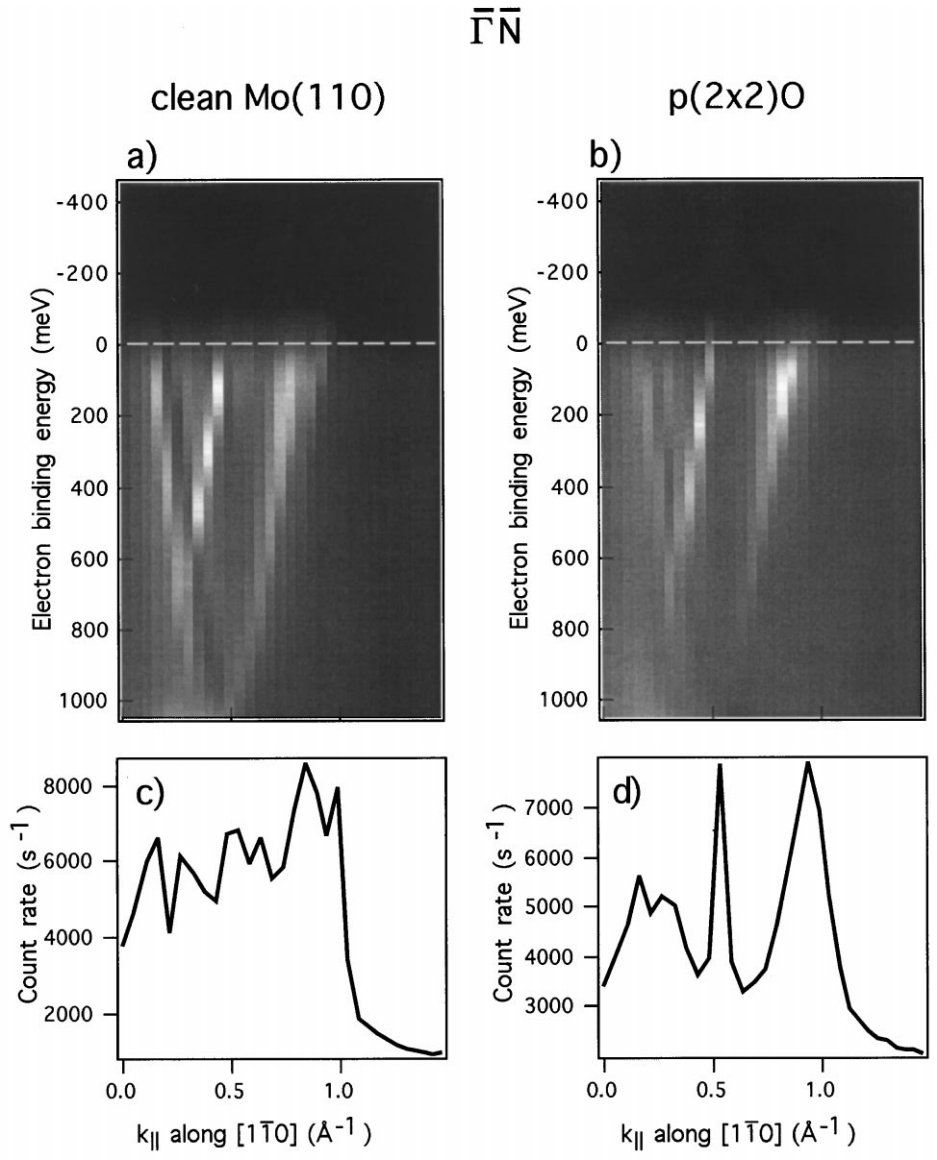

Fig. 6. Analogous to Fig. 5 for the $\bar{\Gamma}\bar{N}$ ([1$\bar{1}$0]) direction.

part of the $\bar{N}$ hole pocket. Upon oxygen adsorption a single band remains, located roughly at the centroid of the former two peaks. Is this an indication for a complete filling of the $\bar{N}$ hole pocket? This question can definitely be negated because there is no down-shifted band that is now completely below E_F.

A similar conclusion can be drawn from the data presented in Fig. 7. For point (3), as mentioned above, we investigated the development of the Fermi surface contours with increasing oxygen coverage. A sequence of Fermi surface maps recorded within the sector of the surface Brillouin zone indicated in Fig. 2a is shown. One can observe that the contour around $\bar{N}$ is shrinking slightly and that it reduces its intensity on the way to the complete p(2 × 2)O. The electron pocket contours become rather diffuse in the intermediate coverage

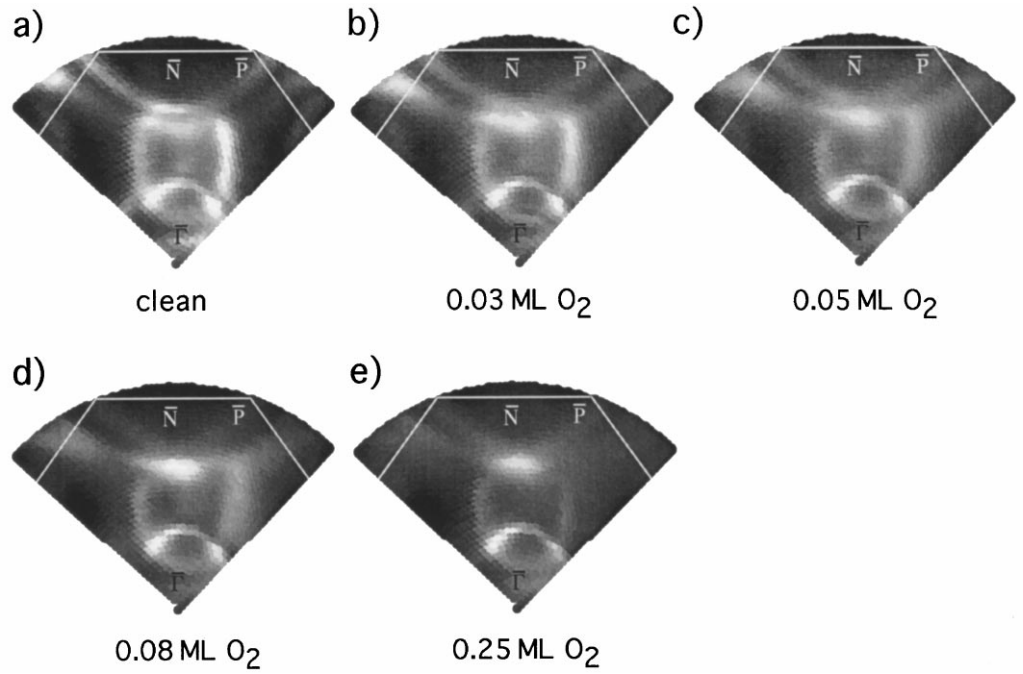

Fig. 7. Development of Fermi surface contour with increasing oxygen coverage for a part of the complete Fermi surface map.

range, finally exposing the almost degenerate bulk state [23] at 0.25 ML coverage, which is again rather sharp in momentum. The question arises of what happened to the surface state electron pocket. We observe neither a continuous shift of its contour such as was seen on the H/Mo(110) adsorbate system [10], nor a gradual build-up of a new contour with increasing oxygen coverage. We can speculate that this state, which is essentially a surface resonance [7], does not feel a strong change in potential due to the oxygen adsorbate, which clearly is located outside the surface. Rather, the outer boundary condition for this surface resonance is changed, thus modifying the reflection coefficient at the surface. The scattering from this state into bulk states might thus be enhanced, providing a natural explanation for the broadening of the associated contours. In the hydrogen case, the adsorbate is located closer to the surface and it can therefore affect the potential seen by the surface resonance more directly. The distance of the hydrogen adsorbate layer at 1 ML coverage to the molybdenum substrate is 1.10 Å [24]. For the oxygen case the authors are not aware of any structural analysis in the literature. The length of the O—Mo bond is in the range of 1.66–2.07 Å [25] and might be expected to be similar to the value obtained for W(110), which is 2.08 Å [26]. This translates into an O—Mo layer distance of $\approx$1.36 Å, which is $\approx$24% larger than in the hydrogen case.

Finally, let us comment on the global Peierls distortion as postulated by Dhar et al. [11] for generating the p(2×2)O superstructure. The main impetus for Dhar et al. to analyse p(2×2)O/Mo(110) was the question why the oxygen adsorbate phases on the (110) surfaces of molybdenum and tungsten differ significantly although both transition metals are very similar. While Mo(110) exhibits a p(2×2)O superstructure at 0.25 ML that fades away for coverages exceeding 0.3 ML in favour of more complex superstructures, W(110) reveals three distinct phases: a (2×1) at 0.5 ML, a (2×2) at 0.75 ML and a (1×1) at 1 ML (see [11] and references therein). Guided by their experimental results, Dhar et al. assert the existence of large elliptical hole pockets around $\bar{N}$ and $\bar{S}$ (see Fig. 2) which allow for global nesting

with a nesting vector that corresponds to the reciprocal vector of the $p(2\times2)$ superstructure. They thus speculate that the oxygen adatoms build the $p(2\times2)$ superstructure by means of a global Peierls distortion. The O/W(110) system, on the contrary, does not reveal similar Fermi surface contours, which consequently does not support such a Peierls-like mechanism for a low-coverage (2×2) phase.

Our photoemission results, however, do not reveal any hint for nested Fermi surface contours, nor do the electron energy-loss spectroscopy data [5,13]: the Rayleigh wave and the longitudinal mode do not suffer any anomalous energy lowering throughout the whole surface Brillouin zone.

4. Summary and conclusion

We have investigated the Fermi surface contours of $p(2\times2)$O/Mo(110) at room temperature. The contours from the oxygen-covered surface essentially reveal a broadening and a reduction in intensity compared with the clean surface. We could not confirm the results of a previous photoemission experiment [11] that reported strong adsorbate-induced changes and largely nested Fermi surface contours. Our results are more consistent with the findings of an electron energy-loss spectroscopy experiment that did not see any anomalous surface phonon softenings that one would expect from a strongly nested Fermi surface.

Acknowledgements

We would like to thank U. Linke for preparing the molybdenum crystal and H. Ibach for kindly placing the crystal at our disposal. We appreciate the help of P. Aebi concerning the construction of a sample holder that allows for heating the crystal to 2000 K. The authors wish to thank W. Deichmann for his support and the mechanical workshop for the technical assistance. This work was supported by the Swiss National Science Foundation.

References

[1] E. Hulpke, J. Lüdecke, Surf. Sci. 287/288 (1993) 837.
[2] E. Hulpke, J. Lüdecke, J. Electron Spectrosc. Relat. Phenom. 64 (56) (1993) 641.
[3] E. Hulpke, in: E. Berthel, M. Donath (Eds.), Electronic Surface and Interface States on Metallic Systems, World Scientific, Singapore, 1995.
[4] J. Kröger, S. Lehwald, H. Ibach, Phys. Rev. B 55 (1997) 10895.
[5] J. Kröger, Dissertation, Rheinisch-Westfälische Technische Hochschule Aachen, D 82, 1998.
[6] B. Kohler, P. Ruggerone, M. Scheffler, Surf. Sci. 368 (1996) 108.
[7] B. Kohler, P. Ruggerone, S. Wilke, M. Scheffler, Phys. Rev. Lett. 74 (1995) 1387.
[8] B. Kohler, P. Ruggerone, M. Scheffler, E. Tosatti, Z. Phys. Chem. 197 (1996) 193.
[9] B. Kohler, Dissertation, Technische Universität Berlin, D 83, 1995.
[10] J. Kröger, T. Greber, J. Osterwalder, Phys. Rev. B (2000) 14146.
[11] S. Dhar, K.E. Smith, S.D. Kevan, Phys. Rev. Lett. 73 (1994) 1448.
[12] S.D. Kevan, in: E. Bertel, M. Donath (Eds.), Electronic Surface and Interface States on Metallic Systems, World Scientific, Singapore, 1995.
[13] J. Kröger, S. Lehwald, H. Ibach, Phys. Rev. B 58 (1998) 1578.
[14] J. Kröger, S. Lehwald, H. Ibach, Surf. Sci. 402–404 (1998) 496.
[15] E. Bauer, H. Poppa, Surf. Sci. 127 (1983) 243.
[16] M.L. Colaianni, J.G. Chen, W.H. Weinberg, J.T. Yates Jr., Surf. Sci. 279 (1992) 211.
[17] T. Greber, O. Raetzo, T.J. Kreutz, P. Schwaller, W. Deichmann, E. Wetli, J. Osterwalder, Rev. Sci. Instrum. 68 (12) (1997) 4549.
[18] K. Jeong, R.H. Gaylord, S.D. Kevan, Phys. Rev. B 39 (1989) 2973.
[19] M. Altman, J.W. Chung, P.J. Estrup, J.M. Kosterlitz, J. Prybyla, D. Sahu, S.C. Ying, J. Vac. Sci. Technol. A 5 (1987) 1045.
[20] J. Osterwalder, Surf. Rev. Lett. 4 (2) (1997) 391.
[21] T.J. Kreutz, T. Greber, P. Aebi, J. Osterwalder, Phys. Rev. B 58 (1998) 1300.
[22] K. Jeong, R.H. Gaylord, S.D. Kevan, Phys. Rev. B 38 (1988) 10302.
[23] E. Rotenberg, J.W. Chung, S.D. Kevan, Phys. Rev. Lett. 82 (1999) 4066.
[24] M. Arnold, S. Sologub, G. Hupfauer, P. Bayer, W. Frie, L. Hammer, K. Heinz, Surf. Rev. Lett. 4 (1997) 1291.
[25] G.A. Somorjai, M.A. Van Hove, Structure and Bonding, Springer, Berlin, 1979.
[26] M.A. Van Hove, S.Y. Tong, Phys. Rev. Lett. (1975) 1092.